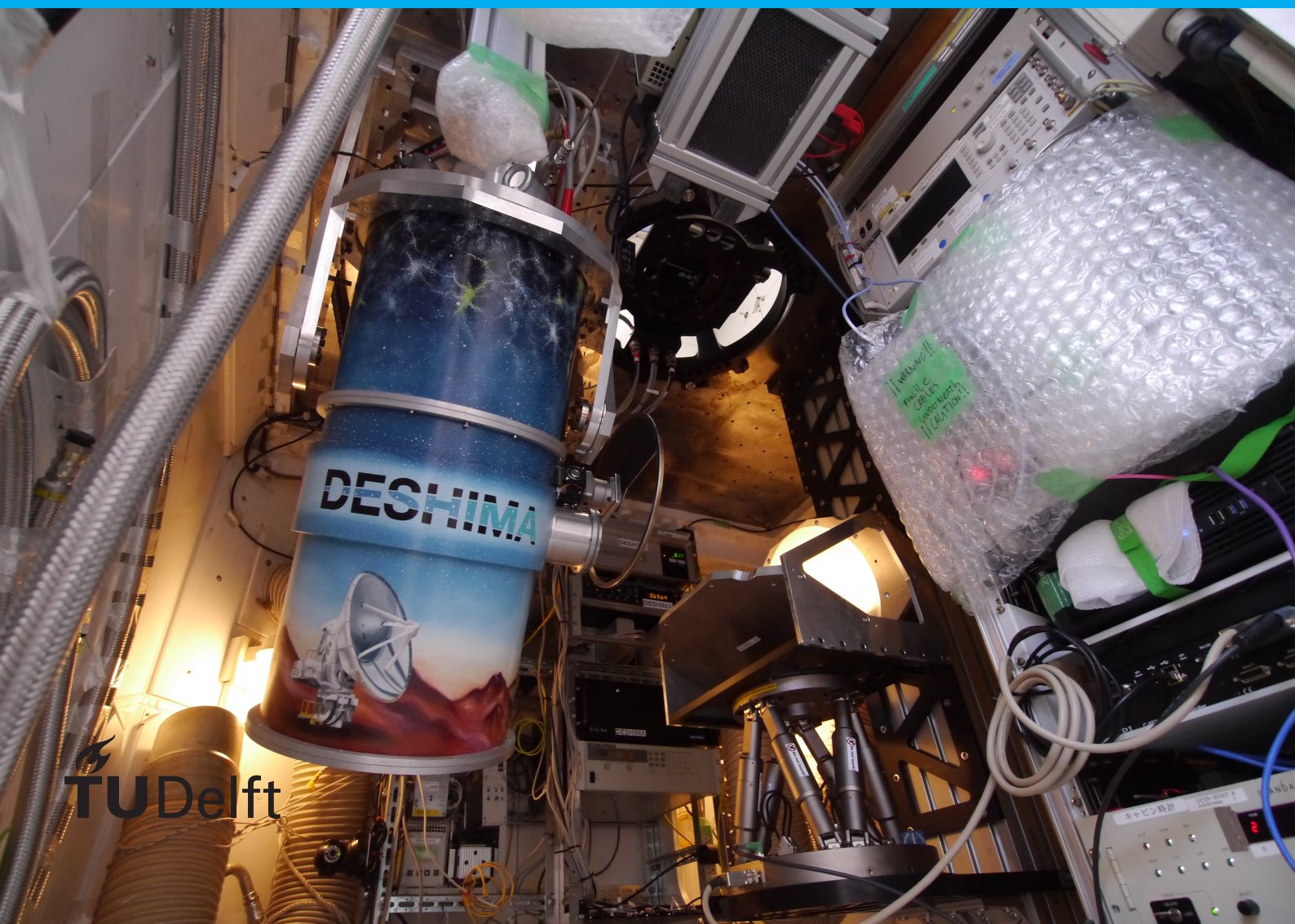


SZFitter

Emilio Amaldi

Predicting DESHIMA 2.0 observations of the thermal Sunyaev-Zel'dovich effect



SZFitter

by

Emilio Amaldi

For the course TN2983 Bachelor Thesis,
as part of the BSc Applied Physics at the Delft University of Technology,
to be defended publicly on Tuesday February 13, 2024 at 13:00.

Student number: 4925343
Project duration: 20 November 2023 - 13 February 2024
Thesis committee: Dr. A. Endo, TU Delft, responsible thesis supervisor
Dr. Kenichi Karatsu, TU Delft, supervisor
Arend Moerman, TU Delft, daily supervisor
Prof. dr. Gary Steele, TU Delft, second examiner

This thesis is confidential and cannot be made public until 13 February 2024

An electronic version of this thesis will be available at <http://repository.tudelft.nl/>.

Cover image by Akira Endo

Contents

Abstract	iv
1 Introduction	1
1.1 Astrophysical context	1
1.2 DESHIMA 2.0	2
1.3 SZFitter	2
2 Methods	5
2.1 Overview of SZFitter	5
2.2 MockSZ	5
2.3 Atmosphere	6
2.4 Filterbank	7
2.5 Noise	9
2.6 Fitting	10
3 Results	13
4 Conclusion and discussion	15

Abstract

Galaxy clusters are some of the largest known structures in the universe. Studying them observationally and theoretically can provide a lot of information on how these clusters form and are structured. One way to study them is through the so-called Sunyaev-Zel'dovich (SZ) effect, which is an interaction between the cosmic microwave background (CMB) and hot electrons in the cluster medium. The SZ effect can be further broken down into a thermal component (tSZ) arising from the random motion of the electrons, and a kinematic component (kSZ) arising from the bulk motion of the cluster medium, making it a good probe for several properties of the cluster.

The SZ effect can be observed as a distortion of the CMB spectrum using submillimeter spectrometry. However, at many submillimeter frequencies radiation is absorbed strongly by the atmosphere. This makes it hard to interpret the measured SZ signal, and measurements require long observation times in order to reach a sufficient signal-to-noise ratio.

In this thesis, we present a framework that simulates a submillimeter spectrometer observation of the tSZ effect including noise factors. It then fits a model tSZ signal to the noisy signal. This allows us to investigate the relation between observation time, noise and retrievability of cluster properties.

We simulate a galaxy cluster with an electron temperature $T_e = 15.3$ keV and central optical depth $\tau_e = 0.0172$ with two simulated DESHIMA-type filterbanks spanning different frequency ranges. For each filterbank we perform 20 simulations with an observation time of 16 hours each, and 20 simulations of 32 hours. We fit every simulation separately, but average over simulations to obtain an expectation value for T_e and τ_e given a filterbank and observation time. We also repeat each fit over rebinned copies of the noisy spectra, combining 7 data points into each bin.

All tested combinations of filterbanks and observation times produce fits with results that are consistent with the input parameters. The 160-320 GHz filterbank consistently gives lower errors than the 220-440 GHz filterbank. From rebinning, we do not find any significant improvement or degradation of the quality of the fits.

The estimates obtained from rebinned data deviate very little from the original estimates, by at most 5%, and show no change in consistency.

From this result, we conclude that SZ observations using DESHIMA 2.0 could provide estimates on cluster parameters. These estimates are already consistent after 16 or 32 hours of observation time. However, we recommend a new filterbank design that covers 160-320 GHz since the error on estimates using this range are smaller than the errors obtained using the original 220-440 GHz filterbank. This is likely due to the atmosphere absorbing much less radiation at this frequency range. Additionally, the results from rebinning show that this new filterbank could contain fewer filters with a lower resolving power without degradation of fit quality.

Introduction

1.1. Astrophysical context

Galaxy clusters are among the largest known structures in the universe. While named for being groupings of large numbers of galaxies, a significant fraction of the cluster's mass resides in the space between galaxies, as a sparse and strongly ionized gas known as the intracluster medium (ICM) [Sparke and Gallagher, 2007].

Of the matter in a galaxy cluster, the ICM is the matter that has not yet been attracted into denser structures by gravity. It has been strongly ionized by radiation from the surrounding galaxies in the period known as the era of reionization, up until about a billion years after the Big Bang [Madau, 2002]. Before galaxies formed however, it was a neutral gas that formed when expansion and cooling from the Big Bang allowed baryons and electrons to form atoms, in a period called the era of recombination [Tanabashi et al., 2018]. As this happened, the Universe changed from an optically opaque plasma into a transparent neutral gas. No longer in a state where matter constantly scattered radiation, the now high-transparent Universe allowed light to travel freely over immense distances. This phase transition is known as decoupling [Birkinshaw, 1999], referring to the decoupling of matter and radiation. Light from this time reaches Earth as the cosmic microwave background (CMB) since the expansion of the Universe has increased its wavelength by over a factor 1000 [Sunyaev, 1974].

On Earth, the CMB is visible as a nearly isotropic and ideal blackbody spectrum [Penzias and Wilson, 1965]. Following its discovery however, the increasing precision of measurements has allowed for the discovery of anisotropies in the CMB spectrum on the order of millikelvins [Fixsen et al., 1997].

One particular distortion in the CMB is caused by the aforementioned intracluster medium and known as the Sunyaev-Zel'dovich (SZ) effect [Sunyaev and Zeldovich, 1970]. Being a hot electron gas, the intracluster medium is able to scatter the incoming CMB photons to higher energies through a process known as inverse Compton scattering [Birkinshaw, 1999]. Like Compton scattering this is a matter-radiation interaction, but it oppositely transfers energy from hot electrons to radiation. CMB photons are effectively 'boosted' by hot electrons, causing a small distortion in the CMB spectrum that looks like a wide trough below 200 GHz and a wide peak at higher energies. The exact shape of this distortion and peak is dependent on several properties of the gas, most notably the electron temperature T_e and the cluster's peculiar velocity relative to the Hubble flow [Birkinshaw, 1999].

There is much yet to discover about the structure and formation of distant galaxy clusters. Observations of the SZ effect promise to provide excellent insight into this, especially when supplemented with data from X-ray observations that study brehmsstrahlung and Comptonization [Birkinshaw, 1999].

A useful and unique property of the Sunyaev-Zel'dovich effect is that it is redshift-independent, meaning that the precise spectrum reaching the observer does not depend on the redshift at which the cluster scatters the CMB. Mathematically speaking, the two different spectral distortions caused by the SZ effect and the expansion of the universe are commutative, and the final distortion of the CMB as it arrives on Earth only depends on the cluster parameters. This makes observation of objects at high redshift almost as easy as at low redshift, in contrast to X-ray observations [Birkinshaw, 1999].

Observations of the SZ effect can be used to absolutely determine electron temperature [Zemcov et al., 2012]. This is highly useful for researching the formation and history of galaxy clusters

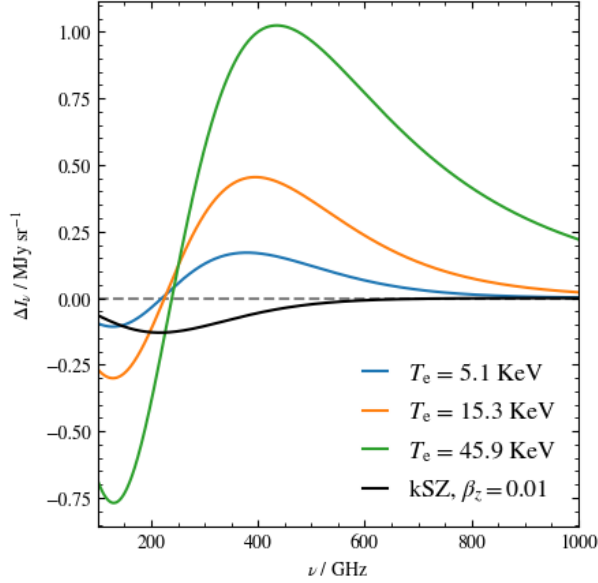


Figure 1.1: Simulated SZ distortion of the CMB generated using MockSZ [Moerman, 2024]. The colored curves are the thermal Sunyaev-Zel'dovich effect, and the black curve is the kinematic SZ effect. The graph displays the SZ distortion of the CMB spectrum without the CMB spectrum itself, which is why some values are negative.

and structures within, based on whether they have reached thermal equilibrium with their surroundings [Mroczkowski et al., 2019]. Knowing the electron temperature of a galaxy cluster, one can also determine the baryonic mass along the line of sight [Birkinshaw, 1999].

There is also a kinematic contribution to the SZ effect [Sunyaev and Zeldovich, 1980] that depends on the peculiar velocity of the cluster relative to the Hubble flow. The kinematic SZ effect is outside the scope of this thesis, but is an important factor since it influences the spectrum considerably. The kinematic SZ effect is useful for studying galaxy clusters' merger history as well as characteristics of the Hubble flow itself, which includes possibly determining the Hubble constant [Birkinshaw, 1999].

1.2. DESHIMA 2.0

The DESHIMA 2.0 spectrometer is an integrated superconducting spectrometer (ISS) built to detect emission lines in dusty star-forming galaxies at high redshift [Rybak et al., 2022]. DESHIMA 2.0 detects light at submillimeter wavelengths over an octave bandwidth (220 GHz-440 GHz) with 347 spectral channels [Taniguchi et al., 2022], see Figure 1.3. The optical chain as part of the Atacama Submillimeter Telescope Experiment (ASTE) 10 m telescope is illustrated in Figure 1.2.

The kinetic inductance detectors (KIDs) in the DESHIMA 2.0 chip are highly sensitive and almost photon-noise limited, although there is some generation-recombination (GR) noise caused by Cooper pairs breaking and recombining in the detectors.

To get as much spectral information from SZ observations as possible, it is desirable to measure over a wide range of frequencies. This could make a wide-band spectrometer like DESHIMA 2.0 suitable for precise SZ measurements. The purpose of this thesis is to simulate SZ observations using DESHIMA 2.0 accounting for sources of noise, and to determine how accurately cluster properties can be retrieved from these measurements. Additionally, we investigate how a similar spectrometer could be designed to optimize for SZ observations specifically.

1.3. SZFitter

To do this, I have written a Python program named SZFitter that simulates observation of the SZ effect using the DESHIMA 2.0 spectrometer. The program obtains an SZ spectrum from the package MockSZ [Moerman, 2024], then simulates atmospheric absorption, the ASTE 10 m telescope and DESHIMA optical chain including a theoretical filterbank. To the simulated output signal I add the amount of noise that would be expected over a given amount of observation time.

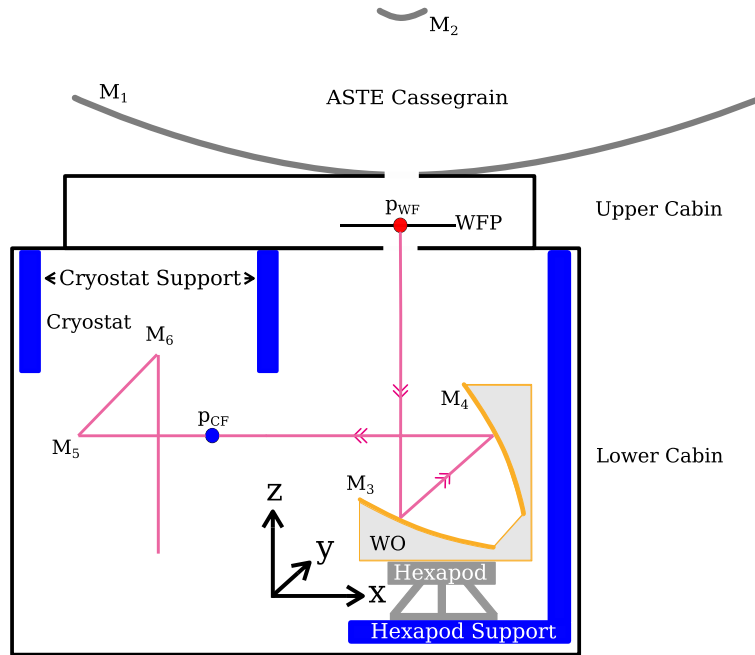


Figure 1.2: The full optical chain for experiments with DESHIMA 2.0. Light from a source is collected at the top by the ASTE Cassegrain telescope dish, which focuses the incoming light into a point in the upper cabin. A so-called “sky-chopper” is placed around this point, that alternatingly switches the telescope beam away from the source and back. Then, a set of adjustable mirrors (the warm optics) in a Dragonian configuration [Dragone, 1978] focus the light into the cryostat, where the chip is housed to make superconductivity possible. Another set of adjustable mirrors direct the light into the chip antenna. Image credit: Arend Moerman.

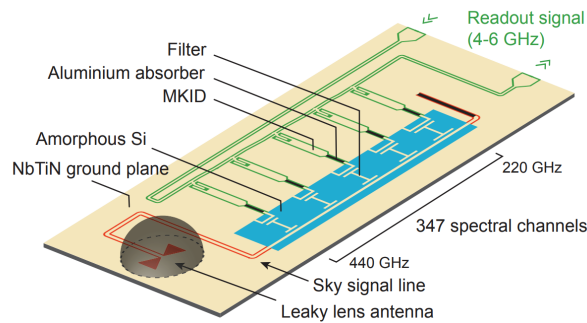


Figure 1.3: Schematic of the chip of the DESHIMA 2.0 spectrometer. The signal enters the chip via the leaky lens antenna and is guided by a waveguide to the filterbank. Each filter channel consists of a band-pass filter and a superconducting kinetic-inductance detector (KID). The readout line then reads out power impinging on each detector. Image taken from [Taniguchi et al., 2022].

Then, the noiseless output curve $P_{SZ}(\nu)$ is fit against the noisy data using a weighted least-squares method. This gives us estimates of the electron temperature T_e and the cluster’s optical depth τ_e . We analyze 20 realizations of noise for filterbanks with different parameters and for observation times of 16 and 32 hours. The observation time is an important factor, since if it would take thousands of hours to obtain a reasonable estimate of the parameters, the viability of the observation comes into question.

The scope of this thesis is limited to the thermal SZ effect and mostly concerned with fitting the electron temperature T_e . For all of this thesis, meaning that the simulated intracluster medium has reached thermal equilibrium [Birkinshaw, 1999], which the fitter also assumes to be the case. More specifically, the relativistic Maxwellian kernel [Rephaeli, 1995] is used.

The theory and methods used for this thesis are described in chapter 2. The results are described in chapter 3 and discussed in chapter 4 along with the conclusions of this thesis.

2

Methods

2.1. Overview of SZFitter

SZFitter is the name of the Python 3 module I created for this project, which is used for all subsequent methods and results unless otherwise noted. In many ways it is a simpler equivalent of the time-dependent simulation software TiEMPO [Huijten, 2020], instead assuming a static atmosphere rather than simulating a dynamic time-dependent one.

In broad terms, the simulation consists of an SZ spectrum generated by MockSZ, atmospheric transmission calculation, a simplified telescope optics chain, a simulated filterbank that represents the DESHIMA 2.0 chip, noise calculation to apply to the power signal and a least-squares fit that fits a noiseless signal curve to the obtained noisy data.

2.2. MockSZ

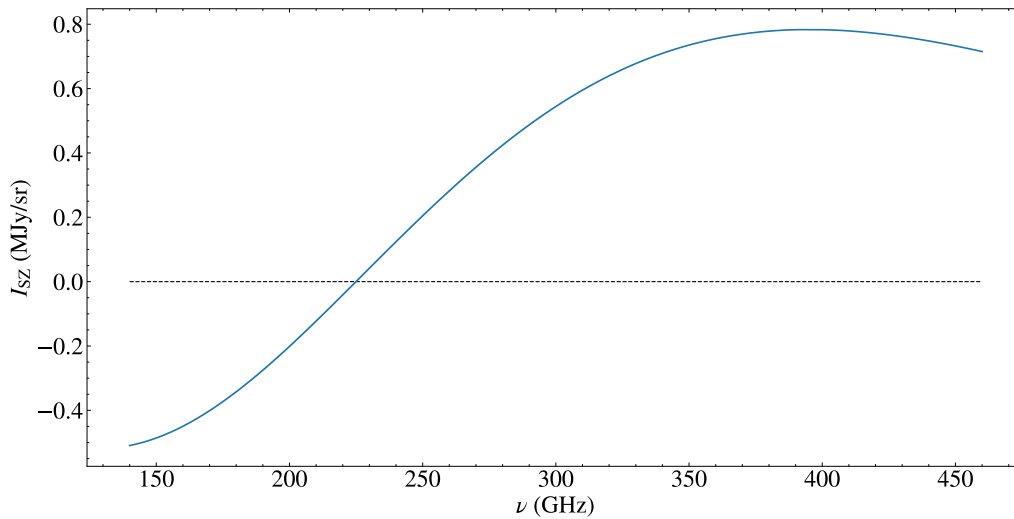


Figure 2.1: Specific intensity of the thermal SZ effect from 140-460 GHz, generated by MockSZ. $T_e = 15.3$ keV. and $\tau_e \approx 0.0172$.

MockSZ [Moerman, 2024] is a Python module made for generating mock maps of the SZ effect in a simulated galaxy cluster. It simulates a relativistic scattering kernel [Rephaeli, 1995] based on the input cluster parameters as well as a CMB spectrum to be scattered by the cluster. Then, MockSZ convolves these to obtain a spectrum in unit of specific intensity. The cluster parameters chosen for this thesis are

loosely based on the galaxy cluster RX J1347.5-1145, which is one of the most massive and luminous galaxy clusters in the sky [Schindler et al., 1996]. Most importantly the input electron temperature T_e is set to 15.3 keV for all simulations in this thesis, and the cluster optical depth $\tau_e \approx 0.0172$.

2.3. Atmosphere

The SZ spectrum generated by MockSZ, $I_{SZ}(\nu)$, is in specific intensity. To correctly run this through the filterbank, it needs to be converted to power spectral density (PSD). At this step we also take into account atmospheric transmission and losses in the optical chain:

$$\text{PSD}_{SZ}(\nu) = \lambda^2 \eta_{\text{chain}} \eta_{\text{atm}}(\nu) \eta_{\text{AP}}(\nu) \cdot I_{SZ}(\nu) \quad (2.1)$$

Here η_{chain} is the product of various frequency-independent transmission efficiencies that each represent a different loss in the optical chain as listed in Table 2.1. Taken together,

$$\eta_{\text{chain}} = \eta_{\text{inst}} \eta_{\text{co}} \eta_{\text{mir}} \eta_{\text{fwd}} \eta_{\text{pol}} \approx 0.091 \quad (2.2)$$

λ is the wavelength of light with frequency ν , note that the factor λ^2 assumes optimal throughput in the antenna. η_{AP} is the aperture efficiency, which represents the fraction of an incoming plane wave from the source that can be coupled to the aperture. This efficiency is frequency-dependent since it is caused in part by the surface roughness of ASTE's reflector dish, which scatters radiation differently depending on its wavelength [Ruze, 1966]. The aperture efficiency only affects the source signal and is given by:

$$\eta_{\text{AP}}(\nu) = \eta_{\text{AP},0} \cdot \exp\left(-\left(\frac{4\pi\epsilon}{\lambda}\right)^2\right) \quad (2.3)$$

Here ϵ is the root mean square (RMS) roughness of ASTE's reflector surface. In our simulation we use $\epsilon = 42$ micron, taken from [Ishii, 2016]. $\eta_{\text{AP},0}$ is the frequency-independent component of the aperture efficiency, and is the product of the taper and spillover efficiencies as described in [Moerman, 2022]

η_{atm} is the strongly frequency-dependent transmission of the atmosphere based on the water vapor content in the sky as described in [Huijten, 2020]. Transmission data is calculated ¹ using the ATM model [Pardo et al., 2001] and displayed in Figure 2.2.

For DESHIMA observations, atmospheric data is taken from the ALMA radiometer [Nikolic et al., 2013] in terms of precipitable water vapor (PWV). For this calculation and for all following simulations, PWV is assumed to be 1.0 mm.

The elevation angle of the telescope beam also matters, since the beam path length through the atmosphere is longer at lower angles. As a result, more radiation is absorbed than what the ALMA radiometer measures at zenith. To generalize this for any angle, we use:

$$\eta_{\text{atm}}(\nu) = \eta_{\text{atm,zenith}}^{\text{csc}(E1)}(\nu) \quad (2.4)$$

Transmission at zenith $\eta_{\text{atm,zenith}}$ is raised to the power of the cosecant of the telescope's elevation angle $E1$. The exponent is approximately 1.15 for an elevation of 60 degrees, which is the elevation used throughout the simulation.

The SZ signal is only a tiny fraction of the radiation that DESHIMA 2.0 measures. DESHIMA's detection range covers many frequencies where Earth's atmosphere is much brighter than the CMB, and even more so than the SZ distortion of the CMB. The total signal PSD_{tot} is dominated by three sources of thermal radiation: PSD_{atm} from the atmosphere, $\text{PSD}_{\text{ground}}$ from the ground and $\text{PSD}_{\text{telescope}}$ from the telescope dish itself. Even at frequencies where η_{atm} is greatest, PSD_{tot} is more than five orders of magnitude greater than PSD_{SZ} . We say that this difference results in the performance of the observation being background limited.

The three thermal effects' PSDs are given by:

$$\text{PSD}_{\text{atm}}(\nu) = \lambda^2 \eta_{\text{chain}} (1 - \eta_{\text{atm}}(\nu)) B_{T_{\text{atm}}}(\nu) \quad (2.5)$$

¹Calculated by <https://www.apex-telescope.org/sites/chajnantor/atmosphere/transpwv/>. Accessed on 30 January 2024.

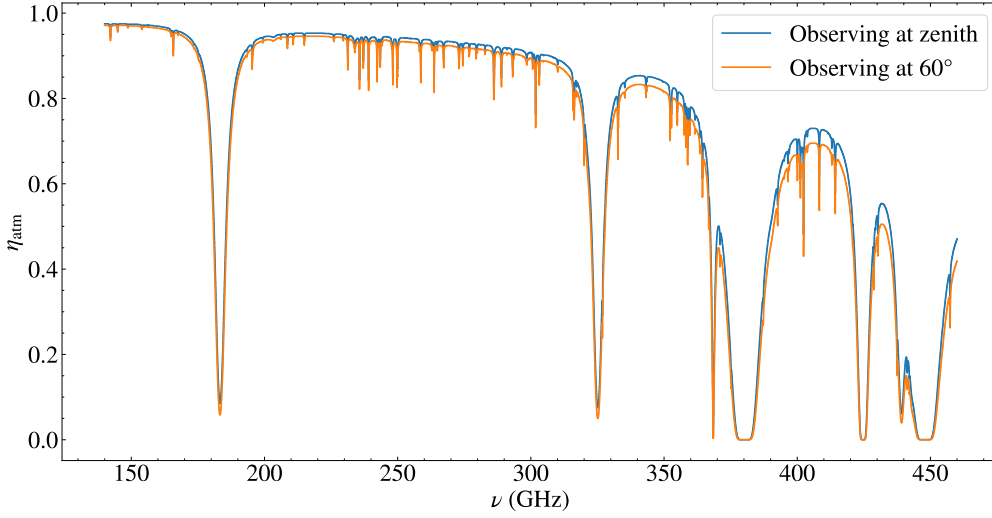


Figure 2.2: Simulated atmospheric transmission η_{atm} due to water vapor content for a PWV of 1.0 mm. The blue line shows atmospheric transmission when the telescope is pointed at zenith, and the orange line is atmospheric transmission at an elevation of 60 degrees.

Table 2.1: An overview of transmission efficiencies in the DESHIMA optical chain, taken from and described in more detail in Huijten [2020]. $\eta_{\text{chain}} = \eta_{\text{inst}}\eta_{\text{co}}\eta_{\text{mir}}\eta_{\text{fwd}}\eta_{\text{pol}}$.

Symbol	Value	Description and cause
η_{inst}	0.35	Instrument efficiency. Losses in the DESHIMA 2.0 chip.
η_{co}	0.65	Cold optics efficiency. Losses in the cryostat.
η_{mir}	0.89	Mirror efficiency. Efficiency of the mirror surfaces.
η_{fwd}	0.90	Forward efficiency. Diffraction losses and fraction of beam that points forward.
$\eta_{\text{AP},0}$	0.66	Aperture efficiency excluding Ruze term. $\eta_{\text{AP},0} = \eta_{\text{taper}}\eta_{\text{spillover}}$
η_{pol}	$\frac{1}{2}$	Polarization efficiency. Incoming light is unpolarized, only half is absorbed.

$$\text{PSD}_{\text{ground}}(\nu) = \lambda^2 \eta_{\text{inst}} \eta_{\text{co}} \eta_{\text{mir}} \eta_{\text{pol}} (1 - \eta_{\text{fwd}}) B_{T_{\text{ground}}}(\nu) \quad (2.6)$$

$$\text{PSD}_{\text{telescope}}(\nu) = \lambda^2 \eta_{\text{inst}} \eta_{\text{co}} \eta_{\text{pol}} (1 - \eta_{\text{mir}}) B_{T_{\text{telescope}}}(\nu) \quad (2.7)$$

Here $B_T(\nu)$ is the specific intensity blackbody spectrum at a temperature T . $T_{\text{atm}} = 273\text{K}$, $T_{\text{ground}} = 280\text{K}$ and $T_{\text{telescope}} = 300\text{K}$ are the temperatures of the atmosphere, ground and telescope respectively. The total power spectral density also includes the ground term and telescope term. Note that the aperture efficiency η_{AP} only applies to the signal PSD [Endo and Baselmans, 2023].

2.4. Filterbank

Analytically, each channel of DESHIMA 2.0 can be modeled as a separate curve $\eta_j(\nu)$. This is a dimensionless efficiency as a function of frequency, where j indexes each spectral channel of the filterbank. The value of $\eta_j(\nu)$ represents how efficiently a monochromatic signal at frequency ν is converted to power in channel j . We model the filters as 350 Lorentzian curves with equal resolving power $R = \frac{\nu_j}{\Delta\nu_j} = 500$ and peak efficiency $\eta_0 = 0.3$. The precise expression is:

$$\eta_j(\nu) = \eta_0 \frac{\gamma^2}{(\nu_j - \nu)^2 + \gamma^2} \quad (2.8)$$

Here, $\gamma_j = \Delta\nu_j/2 = \nu_j/2R$, or half the width of the peak. We want the peak width and the distance between the filter peaks to scale proportionally with frequency: around 220 GHz, the gaps and peaks

are half as wide as at 440 GHz. Since R is constant, the peak width will always be proportional to the center frequency of the filter. The filters are spaced according to resolving power, so the center frequencies of the filters ν_j are defined by:

$$\nu_j = \nu_0 \cdot \left(1 + \frac{1}{R}\right)^j \quad (2.9)$$

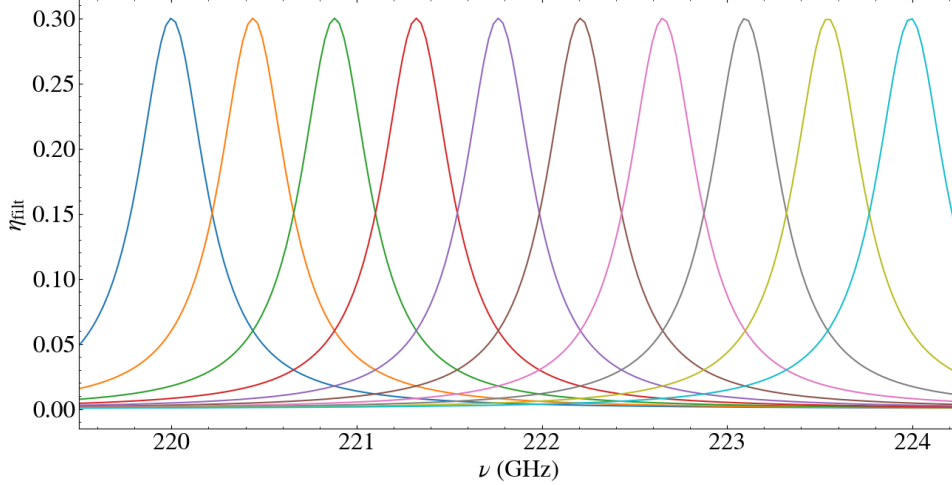


Figure 2.3: The first ten filters of the 220 GHz - 440 GHz filterbank. Note that at every frequency in range, several filters have transmission within an order of magnitude of η_0 .

Because the filter transmissions overlap significantly, even a monochromatic incoming signal will be detected by multiple adjacent filters. An incident spectrum covering the detection range will cause power to impinge on every filter, giving us a signal that is similar in shape to the incoming spectrum. The power in each channel P_j is discretized however, and there is significant cross-talk between adjacent channels. This can be seen as the overlap of the space underneath the curves in Figure 2.3.

Within the simulation, after the incoming signal is transmitted through the filterbank, the power impinging in each channel is associated with the peak frequency of each channel. However, for a faithful reconstruction of the signal one needs to take into account the shape of each filter's response. For example, if power impinges on five adjacent channels, the incoming signal could be monochromatic. SZFitter accounts for the filter curves by including the filterbank operation and atmospheric transmission in the definition of the noiseless curve that is fit to the noisy data points.

DESHIMA 2.0 was built for observing spectral lines in high-redshift galaxies [Taniguchi et al., 2022], and its detection range of 220 to 440 GHz reflects that. This range is quite high for the purpose of SZ observations however, since it does not contain most of the frequencies where the SZ specific intensity is negative, see Figure 2.1. At many of these frequencies, the atmosphere also absorbs nearly all of the light coming from the source, see Figure 2.2. We simulate a second filterbank with a lower frequency range from 160 to 320 GHz, which we expect to require less observation time to estimate the parameters accurately. The resolving power, peak efficiency and number of filters of our simulated filterbanks are the same. The 220-440 GHz filterbank should be functionally identical to the one used in [Tiebosch, 2022].

Now that we have PSD_{SZ} from Equation 2.1 as well as an expression for the filterbank efficiencies, the power impinging by the SZ signal on each detector channel is given by:

$$P_{\text{SZ},j} = \int \eta_{\text{filt},j}(\nu) \text{PSD}_{\text{SZ}}(\nu) d\nu \quad (2.10)$$

For all of the theory described so far, we used analytic expressions of ν . SZFitter discretizes the source frequencies however, as 1500 linearly spaced frequencies ν_i . Along with this, all terms that are

expressed analytically as a function of ν are instead arrays with indices i on one of their dimensions. For example, the 350 filterbank efficiency curves $\eta_j(\nu)$ instead become a large matrix $\eta_{j,i}$ and $eta_{AP}(\nu)$ becomes $eta_{AP,i}$. The filter channel indices are still represented by j .

2.5. Noise

The observation separates the SZ signal from the other sources of radiation using the sky-chopper. Each observation step, the off-source signal is subtracted from the on-source signal. Since the noise is uncorrelated in time, when integrating and averaging over the signal, the signal contribution scales linearly with observation time t_{obs} while the noise contribution scales with $\sqrt{t_{\text{obs}}}$. For a sufficiently long observation time, the SZ signal can then be isolated from the noise terms.

Noise equivalent power (NEP) is defined as the signal power that would be required to give 1:1 signal-to-noise ratio, after 0.5 seconds of integration time. Each channel has its own scalar NEP. For DESHIMA 2.0 observations, this depends on various factors described in more detail in [Tiebosch, 2022]. The full formula is:

$$\text{NEP}_j = \sqrt{2 \int_0^\infty \left(h\nu\eta_{\text{filt},j}(\nu)\text{PSD}(\nu) + \eta_{\text{filt},j}^2(\nu)\text{PSD}^2(\nu) + \frac{2\Delta_{\text{Al}}}{\eta_{\text{pb}}}\eta_{\text{filt},j}(\nu)\text{PSD}(\nu) \right) d\nu} \quad (2.11)$$

The three terms inside the integral correspond to Poisson noise, photon bunching noise and generation-recombination (GR) noise, respectively. This calculation of NEP is identical to that described in [Tiebosch, 2022]. Planck's constant is denoted as h and $\text{PSD}(\nu)$ is the total power spectral density at the detector. The gap energy of aluminium is denoted by $\Delta_{\text{Al}} = 188 \text{ eV}$, and $\eta_{\text{pb}} = 0.4$ is the pair-breaking efficiency.

Each term depends on the total PSD that reaches the filterbank, which is taken as the sum of only the atmosphere, ground and telescope as calculated in Equations 2.5, 2.6 and 2.7. The contribution of the CMB let alone the SZ effect are negligible in comparison. This negligibility holds at every point in time, and the observation time does not change how this influences the NEP. So, we are safe to ignore these terms, simplifying our calculation considerably.

DESHIMA 2.0 is equipped with a so-called sky chopper, which alternates the beam from pointing at the cluster (on-source) and away from it (off-source) to measure the brightness of the atmosphere [Taniguchi et al., 2022]. The atmospheric measurement is then subtracted from the on-source measurement. Integrating this difference over a long enough time will gradually cancel out noise, since the noise is uncorrelated while the SZ signal is continuous.

Due to the sky chopper, on-source integration time is only half of the observation time. Additionally, the atmospheric subtraction requires us to take an additional factor $\sqrt{2}$ into account for the standard deviation of the noise, since the difference between random variables with equal variance is equivalent to a random variable with twice the variance.

To simulate the noise over the integrated power signal, we calculate a standard deviation for each channel by adjusting the NEP to the observation time. This is done assuming a completely stable atmosphere, with constant PWV. A time-dependent simulation of DESHIMA 2.0 observation does exist in the form of TIEMPO [Huijten, 2020], which simulates a dynamic atmosphere and calculates the NEP for each individual integration step. This is not necessary for our purposes since we aren't interested in the time-behavior of the signal, only in the resultant integrated and averaged spectrum at the end of the observation. This is also too computationally expensive for our purposes, as we need to model and fit a large amount of noisy signal realizations to estimate the expected accuracy and precision of our fitting method.

So, the NEP is calculated once for each filter assuming a static atmosphere. The NEP is then adjusted for integration time. This uses half the observation time as integration time and includes the $\sqrt{2}$ factor described above. The standard deviation of noise to add to each channel σ_j is given by:

$$\sigma_j = \sqrt{\frac{0.5 \text{ s}}{t_{\text{obs}}/2}} \sqrt{2\text{NEP}_j} = 2 \sqrt{\frac{0.5 \text{ s}}{t_{\text{obs}}}} \text{NEP}_j \quad (2.12)$$

We then model the noise as a series of independent normally distributed draws with mean 0 and standard deviation σ_j , which we add to the calculated noiseless $P_{\text{SZ},j}$ from Equation 2.10. This can in

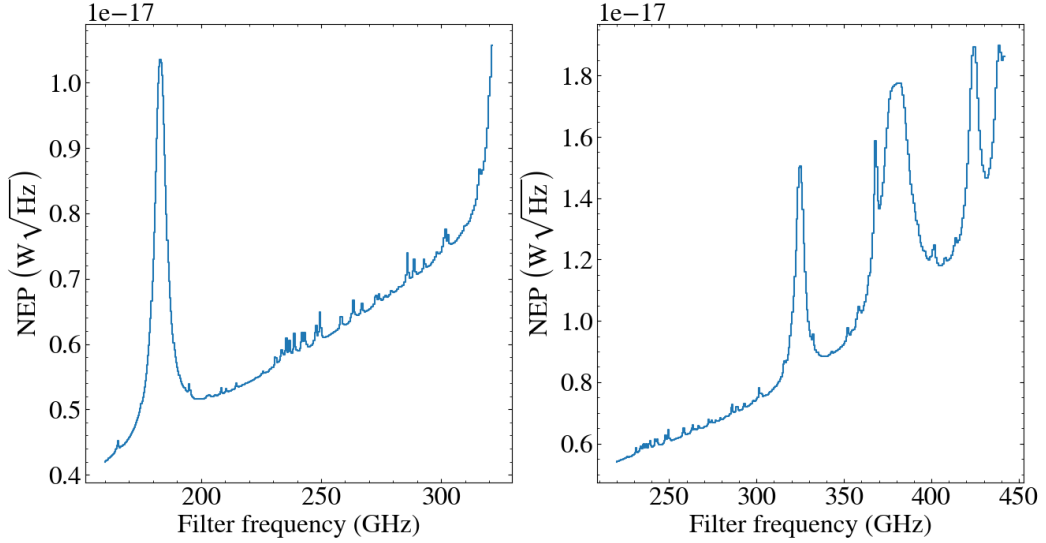


Figure 2.4: The NEP of each channel as a function of frequency for the two different filterbanks.

part be justified again by the fact that SZ signal is over 5 orders of magnitude weaker than the total incoming light.

2.6. Fitting

Then, the Python function `curve_fit` from the package `scipy.optimize` [Virtanen et al., 2020] is used to fit the noiseless $P_{SZ,j}$ curve to the noisy data. The function returns optimal estimates for T_e and τ_e as well as an estimated standard error belonging to these estimates.

I chose to use `scipy.optimize.curve_fit` as it is able to fit any 1-D curve to a set of data points. The $P_{SZ,j}$ curve is somewhat jagged in shape due in large part to the jagged shape of atmospheric transmission, and fitting according to a polynomial or other simple analytical function would not capture the shape of the signal. Another useful feature is that `scipy.optimize.curve_fit` can take an array of measurement uncertainties associated with each data point, for which it will adjust the fit accordingly. We have these in the form of σ_j , which is realistically obtainable in a real life observation since the ALMA radiometer measures PWV. In addition, the NEP does not depend on the unknown cluster parameters since the signal PSD is negligible in comparison to the total PSD.

It is crucial to pass the measurement uncertainties to `curve_fit` due to how different the noise variances are at different filter frequencies. Since this is a least squares fit, large deviations from the curve weigh more negatively toward the score of the fit. For channels that experience the most atmospheric absorption, σ_j is much higher than at frequencies where η_{atm} is high. The signal is attenuated the most strongly and the atmospheric brightness is also highest, doubly lowering the signal-to-noise ratio. If the uncertainties were all taken to be equal, the fit would be dominated by points with an extremely low signal-to-noise ratio. Instead, `curve_fit` assigns weights to the points based inversely on their measurement uncertainty.

Our fitting curve only takes two parameters: electron temperature T_e and optical depth of the SZ effect τ_e . Although `MockSZ` takes several structural parameters as arguments for generating a simulated cluster, in the end these only affect τ_e in different ways. Since the electron temperature is more important, we combine those structural parameters into one optical depth. We compare the two filterbanks at 16 and 32 hours of observation time.

For every noise realization that we analyze, we rebin that data and fit it again. This means that we divide the filterbank into groups of 7 filters each and combine these into bins, by taking the mean of the powers and frequencies. Effectively, we turn 350 filters into 50. Then, we fit a curve that includes the rebinning operation to the rebinned data. We pass rebinned values of σ_j to `curve_fit` as well, although the rebinned standard deviations are actually about $\sqrt{7}$ times smaller than the original ones

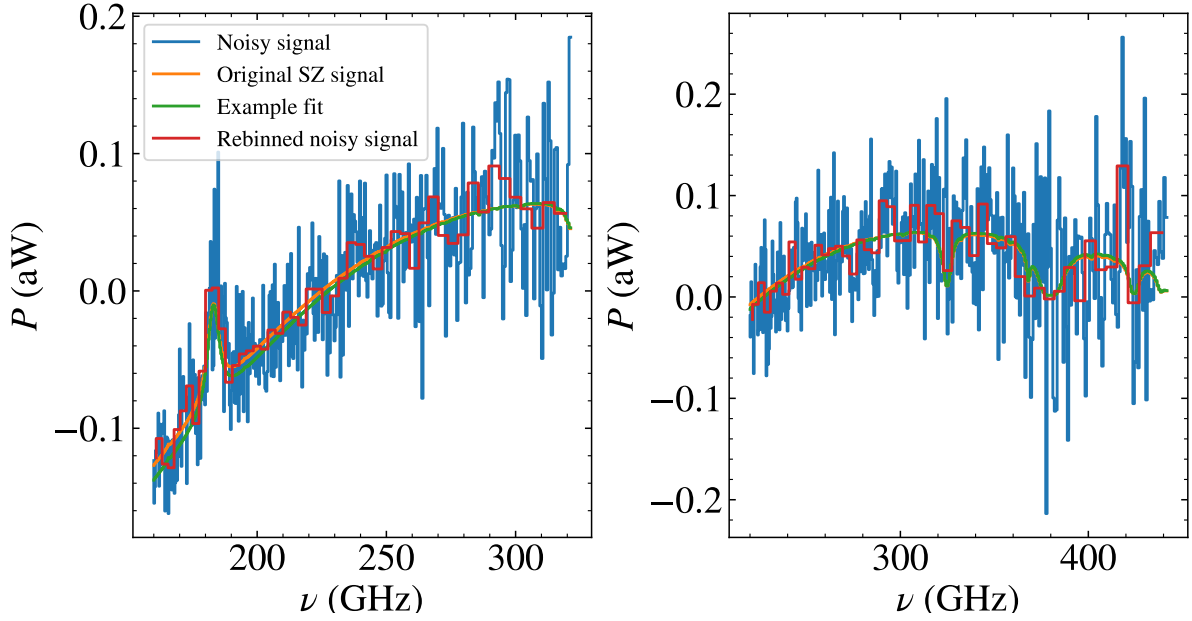


Figure 2.5: Power in each channel, for an observation time of 16 hours and for both filterbanks. The left and right graph use independent noise realizations. The curves in each plot correspond to noisy power, P_{SZ} without noise, a potential fit with arbitrarily chosen parameters $T_e = 7 \text{ keV}$, $\tau_e = 0.03$ and the noisy signal rebinned combining 7 channels into each bin.

due to the way averaging over random variables reduces their variance. This can clearly be seen in Figure 2.5

Rebinning the signal is roughly equivalent to having fewer filters with lower resolving power R and therefore a wider peak. If this yields similar or better results, it would mean that our proposed filterbank could contain far fewer filters, which would make manufacturing the chip less costly and labor-intensive as well as reducing cross-talk between channels in the readout [Li et al., 2022].

Outside of the scope of this thesis are fitting for structural parameters using a scan of pointings over the cluster instead of a single pointing. More research can also be done about the kSZ effect, by fitting for peculiar velocity as well as electron temperature. The thermal SZ effect also exists in non-thermalised hot electron populations, such as the jet of a quasar. This would involve using a so-called power law scattering kernel rather than the relativistic Maxwellian kernel [Birkinshaw, 1999]. It should be noted that MockSZ is able to generate SZ spectra using a power law scattering kernel as well as a kinematic component.

3

Results

All data in this chapter were generated using identical parameters except for observation time and filterbank range. The values for all parameters are described in Chapter 2.

In the following figures, the blue marks with error bars represent the parameter estimates of the noiseless $P_{SZ,j}$ curve when fit to the noisy data. The error bars indicate one standard deviation as given by `curve_fit`. The input parameters are $T_e = 15.3\text{keV}$ and $\tau_e = 0.0172$, indicated by the orange horizontal lines. The estimates of T_e are noticeably inversely related to the optical depth estimates: the path that the T_e estimates trace is very similar to the path that the τ_e estimates do, but flipped vertically. Both parameters contribute positively to the specific intensity spectrum and therefore impinged power, so the estimates' deviations from the input parameters are more likely to be of opposite sign. Balancing them in this way results in a curve closer to the input curve, usually resulting in a better fit.

All plots show the estimates obtained without rebinning. The rebinned results aren't included in the graphs because they are too similar to visibly tell apart. For the 160-320 GHz filterbank, the rebinned estimates deviate less than 0.8% from the non-rebinned estimates on average and are closer to the input parameters about as often as they are less close. For the 220-440 GHz filterbank the differences average up to 5%, but there is still no clear improvement or deterioration of parameter estimation.

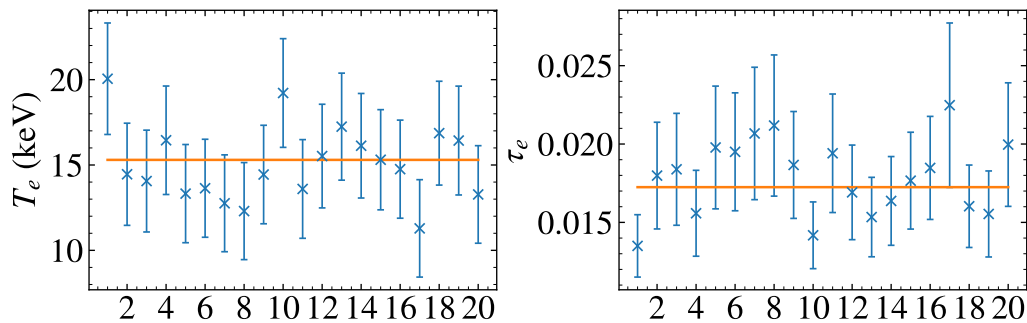


Figure 3.1: The parameter estimates for 16 hour observations using the 160-320 GHz filterbank. The left graph shows estimates of T_e , and the right graph shows estimates of τ_e for the same noise realizations. The error bars are 1σ as given by `curve_fit`.

For all combinations of filterbank and observation time, the T_e parameter estimates are consistent within 2σ . The deviations are significantly lower for the 160-320 GHz filterbank at both observation times. Higher observation time reduces the error in the estimates for both filterbanks.

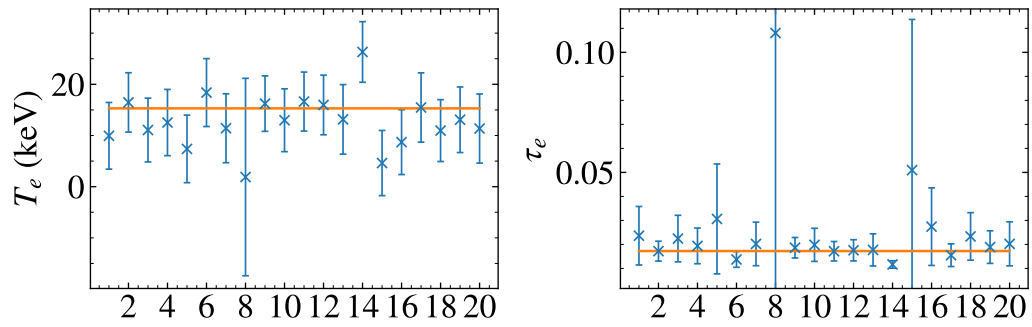


Figure 3.2: The parameter estimates for 16 hour observations using the 220-440 GHz filterbank. The left graph shows estimates of T_e , and the right graph shows estimates of τ_e for the same noise realizations. The error bars are 1σ as given by `curve_fit`.

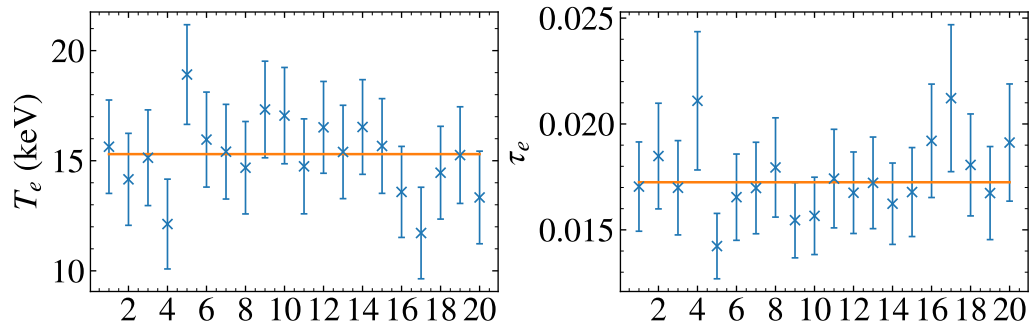


Figure 3.3: The parameter estimates for 32 hour observations using the 220-440 GHz filterbank. The left graph shows estimates of T_e , and the right graph shows estimates of τ_e for the same noise realizations. The error bars are 1σ as given by `curve_fit`.

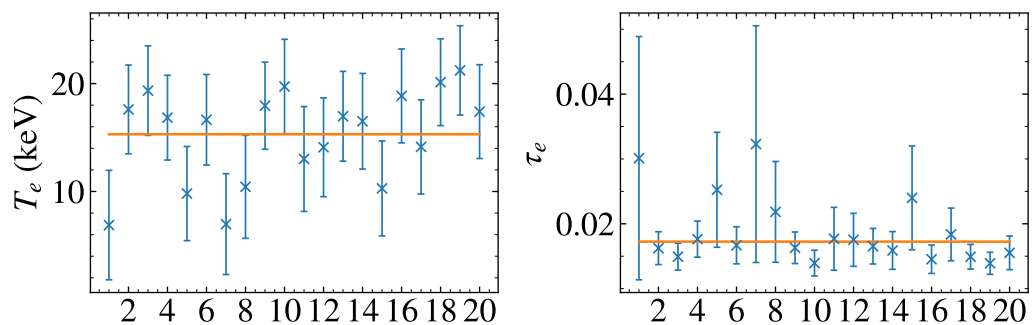
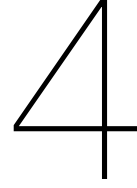


Figure 3.4: The parameter estimates for 32 hour observations using the 160-320 GHz filterbank. The left graph shows estimates of T_e , and the right graph shows estimates of τ_e for the same noise realizations. The error bars are 1σ as given by `curve_fit`.



Conclusion and discussion

Determining the electron temperature and electron optical depth in a single pointing of a galaxy cluster is possible for observation times of 16 and 32 hours using our simulated DESHIMA 2.0 spectrometer. The alternative 160-320 GHz filterbank results in significantly smaller deviations from the input parameters however. As expected, observing for 32 hours results in smaller errors in cluster parameter estimates than observing for 16 hours.

To improve the quality of the fit, this data could be supplemented using ALMA observation data of the same cluster at lower frequencies [Kitayama et al., 2016]. Additionally, X-ray observations of galaxy clusters can determine the Compton y factor, which constrains the relation between T_e and τ_e [Sampoorna, 2009].

In the theory used in our simulation, the SZ effect is modeled as a distortion of the CMB. The CMB is modeled as being at a constant temperature, but in reality the CMB radiation comes from all directions around the cluster at large distances. The CMB is known to be anisotropic in temperature [Fixsen et al., 1997], so in practice there would be variations in the spectra reaching the cluster before scattering toward the observer. The simulation could be improved by modeling a temperature-dependent CMB illuminating the cluster, taking into account the anisotropies.

The function used to generate the noiseless spectrum is effectively identical to the one used to fit the noisy spectrum. This likely favors the accuracy of the fit in a way that wouldn't apply when used on observational data.

Rebinning barely affects the fit parameter estimates. Since rebinning the data is roughly equivalent to having fewer filters with a smaller resolving power, a spectrometer designed for SZ observations could have a factor 7 fewer channels and a factor 7 smaller resolving power. This makes such a spectrometer easier to manufacture, and would also reduce cross-talk in the spectrometer readout line.

While currently limited in scope to the thermal SZ effect, SZFitter could easily be modified to include a peculiar velocity parameter. This would make fitting more difficult, as has been confirmed in a small-scale test that included this modification. In practice however, sources are likely to have some peculiar velocity with respect to the Hubble flow, so v_{pec} would need to be taken into account regardless of whether one wants to determine its value. This deterioration might be compensated for by including information from the aforementioned radio and X-ray observations, however.

Bibliography

- Mark Birkinshaw. The Sunyaev-Zel'dovich Effect. *Physics Reports*, 310(2-3):97–195, 1999. doi: 10.1016/S0370-1573(98)00080-5. URL [https://www.doi.org/10.1016/S0370-1573\(98\)00080-5](https://www.doi.org/10.1016/S0370-1573(98)00080-5).
- C. Dragone. Offset multireflector antennas with perfect pattern symmetry and polarization discrimination. *Bell System Technical Journal*, 57(7):2663–2684, September 1978. ISSN 0005-8580. doi: 10.1002/j.1538-7305.1978.tb02171.x. URL <http://dx.doi.org/10.1002/j.1538-7305.1978.tb02171.x>.
- Akira Endo and Jochem Baselmans. Superconducting astronomical instrumentation lecture notes, lecture 4, slide 4, 2023.
- D. J. Fixsen, G. Hinshaw, C. L. Bennett, and J. C. Mather. The spectrum of the cosmic microwave background anisotropy from the combined COBE FIRAS and DMR observations. *The Astrophysical Journal*, 486(2):623–628, September 1997. ISSN 1538-4357. doi: 10.1086/304560. URL <http://dx.doi.org/10.1086/304560>.
- Esmee Huijten. TIEMPO: Time-Dependent End-to-End Model for Post-process Optimization of the DESHIMA Spectrometer. December 2020. URL <http://resolver.tudelft.nl/uuid:5302e10e-3b56-4d4d-a1fd-6a1d58f57abd>.
- Shun Ishii. Aste efficiencies, 2016.
- Tetsu Kitayama et al. The sunyaev–zel'dovich effect at 5": Rx j1347.5–1145 imaged by ALMA. *Publications of the Astronomical Society of Japan*, 68(5), September 2016. ISSN 0004-6264. doi: 10.1093/pasj/psw082. URL <http://dx.doi.org/10.1093/pasj/psw082>.
- J. Li et al. Reducing frequency scatter in large arrays of superconducting resonators with inductor line width control. *Journal of Low Temperature Physics*, 209(5–6):1196–1203, November 2022. ISSN 1573-7357. doi: 10.1007/s10909-022-02893-8. URL <http://dx.doi.org/10.1007/s10909-022-02893-8>.
- Piero Madau. The era of reionization. 2002.
- A. Moerman. MockSZ, 2024. URL <https://zenodo.org/doi/10.5281/zenodo.8365066>.
- Arend Moerman. Evaluation and characterization of the deshima optics chain, 2022.
- Tony Mroczkowski et al. Astrophysics with the spatially and spectrally resolved sunyaev-zeldovich effects: A millimetre/submillimetre probe of the warm and hot universe. *Space Science Reviews*, 215(1), February 2019. ISSN 1572-9672. doi: 10.1007/s11214-019-0581-2. URL <http://dx.doi.org/10.1007/s11214-019-0581-2>.
- B. Nikolic, R. C. Bolton, S. F. Graves, R. E. Hills, and J. S. Richer. Phase correction for ALMA with 183 GHz water vapour radiometers. *Astronomy and Astrophysics*, 552:A104, April 2013. ISSN 1432-0746. doi: 10.1051/0004-6361/201220987. URL <http://dx.doi.org/10.1051/0004-6361/201220987>.
- J.R. Pardo, J. Cernicharo, and E. Serabyn. Atmospheric transmission at microwaves (atm): an improved model for millimeter/submillimeter applications. *IEEE Transactions on Antennas and Propagation*, 49(12):1683–1694, 2001. ISSN 0018-926X. doi: 10.1109/8.982447. URL <http://dx.doi.org/10.1109/8.982447>.

- A. A. Penzias and R. W. Wilson. A measurement of excess antenna temperature at 4080 mc/s. *The Astrophysical Journal*, 142:419, July 1965. ISSN 1538-4357. doi: 10.1086/148307. URL <http://dx.doi.org/10.1086/148307>.
- Yoel Rephaeli. Cosmic microwave background comptonization by hot intracluster gas. *The Astrophysical Journal*, 445:33, May 1995. ISSN 1538-4357. doi: 10.1086/175669. URL <http://dx.doi.org/10.1086/175669>.
- J. Ruze. Antenna tolerance theoryࣘa review. *Proceedings of the IEEE*, 54(4):633–640, 1966. ISSN 0018-9219. doi: 10.1109/proc.1966.4784. URL <http://dx.doi.org/10.1109/PROC.1966.4784>.
- M. Rybak, T. Bakx, J. Baselmans, K. Karatsu, K. Kohno, T. Takekoshi, Y. Tamura, A. Taniguchi, P. van der Werf, and A. Endo. Deshima 2.0: Rapid redshift surveys and multi-line spectroscopy of dusty galaxies. *Journal of Low Temperature Physics*, 209(5–6):766–778, May 2022. ISSN 1573-7357. doi: 10.1007/s10909-022-02730-y. URL <http://dx.doi.org/10.1007/s10909-022-02730-y>.
- M Sampoorna. Compton scattering in astrophysics. 2009.
- S Schindler, M Hattori, DM Neumann, and H Böhringer. Rosat/hri and asca observations of the most luminous x-ray cluster rxj1347. 5-1145. *arXiv preprint astro-ph/9603037*, 1996.
- Linda S Sparke and John S Gallagher. *Galaxies in the Universe*. Cambridge University Press, Cambridge, England, 2 edition, February 2007.
- R. A. Sunyaev. *The Thermal History of the Universe and the Spectrum of Relic Radiation*, page 167–173. Springer Netherlands, 1974. ISBN 9789401022200. doi: 10.1007/978-94-010-2220-0_14. URL http://dx.doi.org/10.1007/978-94-010-2220-0_14.
- R. A. Sunyaev and Ya. B. Zeldovich. Small-scale fluctuations of relic radiation. *Astrophysics and Space Science*, 7(1):3–19, April 1970. ISSN 1572-946X. doi: 10.1007/bf00653471. URL <http://dx.doi.org/10.1007/BF00653471>.
- R. A. Sunyaev and Ya. B. Zeldovich. The velocity of clusters of galaxies relative to the microwave background. the possibility of its measurement. *Monthly Notices of the Royal Astronomical Society*, 190(3):413–420, March 1980. ISSN 1365-2966. doi: 10.1093/mnras/190.3.413. URL <http://dx.doi.org/10.1093/mnras/190.3.413>.
- M. Tanabashi et al. Review of particle physics. *Physical Review D*, 98(3), August 2018. ISSN 2470-0029. doi: 10.1103/physrevd.98.030001. URL <http://dx.doi.org/10.1103/PhysRevD.98.030001>.
- Akio Taniguchi et al. Deshima 2.0: Development of an integrated superconducting spectrometer for science-grade astronomical observations. *Journal of Low Temperature Physics*, 209(3–4):278–286, November 2022. ISSN 1573-7357. doi: 10.1007/s10909-022-02888-5. URL <http://dx.doi.org/10.1007/s10909-022-02888-5>.
- J. Tiebosch. Photon-bunching in ground-based submillimeter-wave astronomy, 2022. URL <http://resolver.tudelft.nl/uuid:7d150ea8-1cdd-4584-a99e-65392599bfb9>.
- Pauli Virtanen et al. SciPy 1.0: Fundamental Algorithms for Scientific Computing in Python. *Nature Methods*, 17:261–272, 2020. doi: 10.1038/s41592-019-0686-2.
- M. Zemcov et al. High spectral resolution measurement of the sunyaev–zeldovich effect null with z-spec. *The Astrophysical Journal*, 749(2):114, March 2012. ISSN 1538-4357. doi: 10.1088/0004-637x/749/2/114. URL <http://dx.doi.org/10.1088/0004-637X/749/2/114>.